Applied Surface Science 473 (2019) 203–208

Contents lists available at ScienceDirect

Applied Surface Science

journal homepage: www.elsevier.com/locate/apsusc

Full Length Article

Hydrogen intercalation of CVD graphene on germanium (001) – Strain and doping analysis using Raman spectroscopy

Jarosław Judek[a,*], Iwona Pasternak[a], Pawel Dabrowski[b], Wlodek Strupinski[a], Mariusz Zdrojek[a]

[a] Faculty of Physics, Warsaw University of Technology, Koszykowa 75, 00-662 Warszawa, Poland
[b] Department of Solid States Physics, Faculty of Physics and Applied Informatics, University of Lodz, Pomorska 149/153, 90-236 Lodz, Poland

ARTICLE INFO

Keywords:
Graphene on germanium
Hydrogen intercalation
Raman spectroscopy

ABSTRACT

We report a study of structural properties of graphene grown on germanium (001) when subjected to hydrogen intercalation during cooling, using chemical vapor deposition method. The systematic statistical analysis of the Raman spectra indicated that hydrogen increased the number of structural defects in graphene and caused the increase of the compressive strain. Interestingly, it was also found that hydrogen impacted on charge doping. These findings offer a new insight into the nature of graphene-germanium interaction and constitutes an important step towards graphene integration into modern electronics.

1. Introduction

Nowadays, the most popular graphene production method is the chemical vapor deposition (CVD) on copper foils [1]. Whereas the CVD is a feasible, relatively cheap, and large-scale production process, the copper substrate used for this process significantly hinders graphene integration into modern, mostly silicon, electronics [2]. Compatibility with the CMOS technology is one of the most important arguments in a discussion on graphene opto-electronic applications because processes that could not be integrated with modern silicon technological lines will significantly increase the production costs or even render graphene implementation unprofitable. Due to the fact that direct growth of graphene on silicon is impossible as it forms carbides, germanium as a substrate, which is already compatible with silicon based technologies, is an interesting alternative. To date, despite many efforts [3–8], the CVD growth of graphene on germanium remains still to be fully understood and Raman spectroscopy is one of the most powerful techniques that can further aid this purpose.

Generally, in the context of graphene-germanium synthesis basic Raman studies were applied to confirm the correctness of the growth procedures, i.e. to verify the presence of the graphene layer on germanium substrates [3,4,7]. Additionally, more advanced Raman inspections were used to demonstrate and explain the difference between the epitaxial growth of graphene on two crystallographic orientations of the substrate, namely Ge(111) and Ge(110) [6]. This article claims that the thermal postprocessing of GR/Ge(111) and GR/Ge(110) systems under UHV leads to the emergence of new reconstructions of the Ge (111) and Ge(110) surfaces, thus leading to the strain modification of the overlying graphene lattice [9]. Following the work of Kiraly et al., a few other papers, by plotting the distribution of the 2D mode position vs the measured distribution of the G mode position, have shown the estimation of the doping or strain levels in graphene grown on germanium substrates [10–12]. In all of these papers, researchers revealed the presence of a compressive biaxial strain, comparable to the value ($\varepsilon \approx -0.3\%$) present in graphene grown on Ge(100) substrate by the CVD method. Furthermore, this finding is highly valuable as it suggests that CVD growth process of graphene on Ge(100) could be uninfluenced by the growth system. The literature overview also indicates that there is a scarcity of an in-depth study employing Raman spectroscopy characterization, especially in the statistical approach. Interestingly, although researchers conducted their investigations on the post-processed graphene/germanium samples, there are no reports of the advanced correlation of Raman characteristics of hydrogen-intercalated graphene grown on germanium, particularly in the function of the measurement temperature [6,13]. Also, even in the case of widely studied graphene/SiC hydrogen intercalated systems, the studies embracing statistical Raman analysis of temperature dependence hydrogen intercalations are rather rare [14].

Therefore, here we, investigate how the postprocessing, namely hydrogen intercalation in different temperatures during cooling after CVD growth, influences properties of CVD grown graphene on germanium (001) substrate. We use Raman spectroscopy and vector decomposition method [9] to obtain strain ε and doping n values that characterize intercalated in different temperatures graphene monolayers.

* Corresponding author.
E-mail address: jaroslaw.judek@pw.edu.pl (J. Judek).

https://doi.org/10.1016/j.apsusc.2018.12.104
Received 23 August 2018; Received in revised form 30 November 2018; Accepted 12 December 2018
Available online 12 December 2018
0169-4332/

We demonstrate that hydrogen intercalation leads to an increase in compressive strain ε, which is an unexpected effect, and slightly deteriorates structural quality of graphene. In addition, we found slight lower variation of the doping level for all intercalated samples, as compared to pristine one. Our findings and conclusions offer new insight into graphene-germanium interactions in the presence of hydrogen and could be especially useful for further optimization of graphene on germanium technology. We also note that the post-growth hydrogen treatment could be used for strain control, which might be attractive considering that imperfect (defected, strain-disturbed) graphene has been reported to possess some unique functionality [15,16], despite a decrease in the carrier mobility μ value [17].

2. Material and methods

We used commercially available silicon (001) wafer with a 3 μm-thick germanium film deposited on it as a substrate for CVD growth of graphene monolayer and its further hydrogen intercalation. The germanium film was deposited using CVD method and is oriented along (001) crystallographic axis. The substrate surface pretreatment and subsequent graphene growth process were described in Ref. [7]. After the growth, some of the samples were cooled down in pure argon atmosphere (p = 800 mbar) and the others in pure hydrogen (p = 800 mbar, also). We note that the samples cooled down in argon are fabricated using the same procedure as described in Ref [7] are here denoted as “pristine”. Schematic of the cooling procedure for pristine samples is shown in Fig. 1a. Samples that were exposed to hydrogen during cooling are further denoted as “hydrogenated”. Schematic of the cooling procedure for one of the hydrogenated samples is shown in Fig. 1c. The cooling took place in argon between the temperatures of the graphene growth and the hydrogen exposure starting temperature. Next, depending on the process used, starting from T = 600 °C, 800 °C, or 900 °C the samples were cooled down in hydrogen. At the temperature below 500 °C hydrogen was switched again to argon and the cooling was continued until the sample reached room temperature. Immediately after the growth, samples were inspected using scanning electron microscopy and examined using Raman spectroscopy. We observed a progressive degradation of our samples, and therefore, the measurements were performed just after the growth.

Fig. 1b shows scanning electron microscopy (SEM) image of a pristine graphene monolayer on germanium (001) surface, and Fig. 1d shows a SEM image of graphene after hydrogen treatment. A characteristic highly faceted structure [18–20] related to the germanium surface reconstruction is clearly seen for pristine graphene but it is not present on hydrogenated samples. Because the structure of facets were reported to be dependent on the cooling rate [18], we checked if different cooling times of pristine samples affect facet structure, particularly, if it is possible to obtain flat and uniform surface like in the case of hydrogenated samples. Our experiments showed that despite different cooling schemes in pure argon atmosphere, facet structure remained the same. Thus, lack of facet structure in hydrogenated samples is not an effect of different cooling rates/times it is entirely the effect of exposure to hydrogen. This conclusion is in agreement with our previously reported work by Grzonka et al. [21].

In order to support the main analysis of this work the graphene properties were verified by means of low-energy electron diffraction (LEED) and Atomic Force Microscopy (AFM). The LEED measurements were conducted at room temperature under the base pressure of 2×10^{-10} mbar employing a Multiprobe P system made by Omicron GmbH (currently known as Scienta-Omicron). The AFM Measurements were performed in ambient conditions with the Ntegra Aura (NT-MDT).

As presented in Fig. 2a pristine sample without hydrogen intercalation have complex LEED pattern. We are dealing with two different planar graphene domains orientations (denoted by blue and red hexagons) and with different domain alignments relative to the surface which are visible as pairs of blue and red hexagons due to presence of nanofacets structure [11]. After hydrogen intercalation surface can be flattened which results in the presence of only two main planar domain orientation (see Fig. 2b). However, it should be noted that in both cases the orientations of domains are not perfectly defined, as visible spots were significantly blurred and show a tendency to form a ring. In conclusion, the parallel domains orientation does not change after intercalation process and main changes were related to the change in the substrate roughness.

Atomic force microscopy measurements performed on sample without hydrogen revealed that the graphene/Ge(001) was completely covered with nanofacets (Fig. 2c). In the case of sample after hydrogen intercalation we see that the surface is much flatter and nanofacets were almost removed (Fig. 2d) which is consistent with our SEM and LEED measurements.

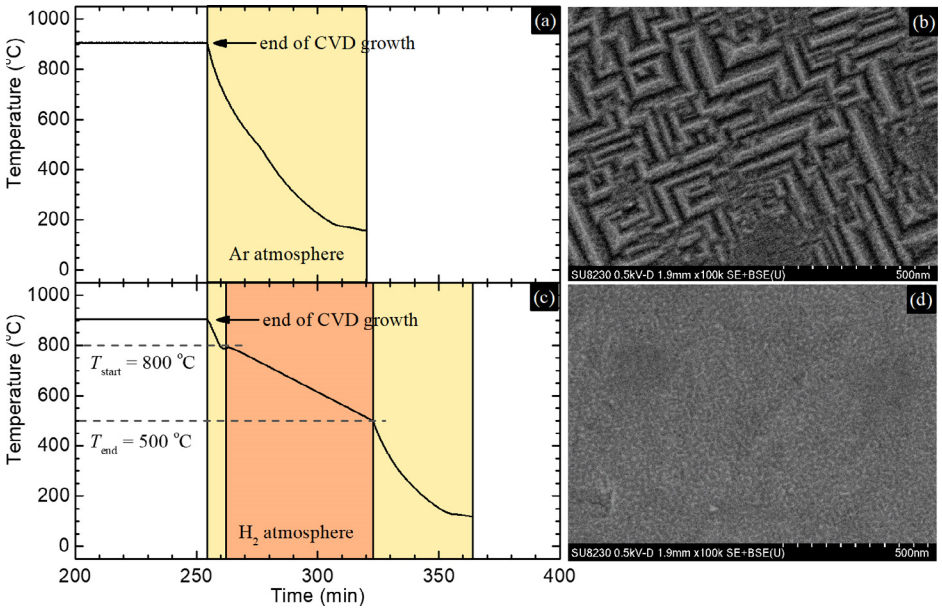

Fig. 1. Scheme of cooling after CVD growth of (a) pristine and (c) hydrogen treated graphene monolayer on germanium (100) substrate. (b) SEM image illustrating graphene before hydrogenation, graphene reflects germanium surface reconstruction, and (d) SEM image illustrating graphene surface after hydrogen treatment.

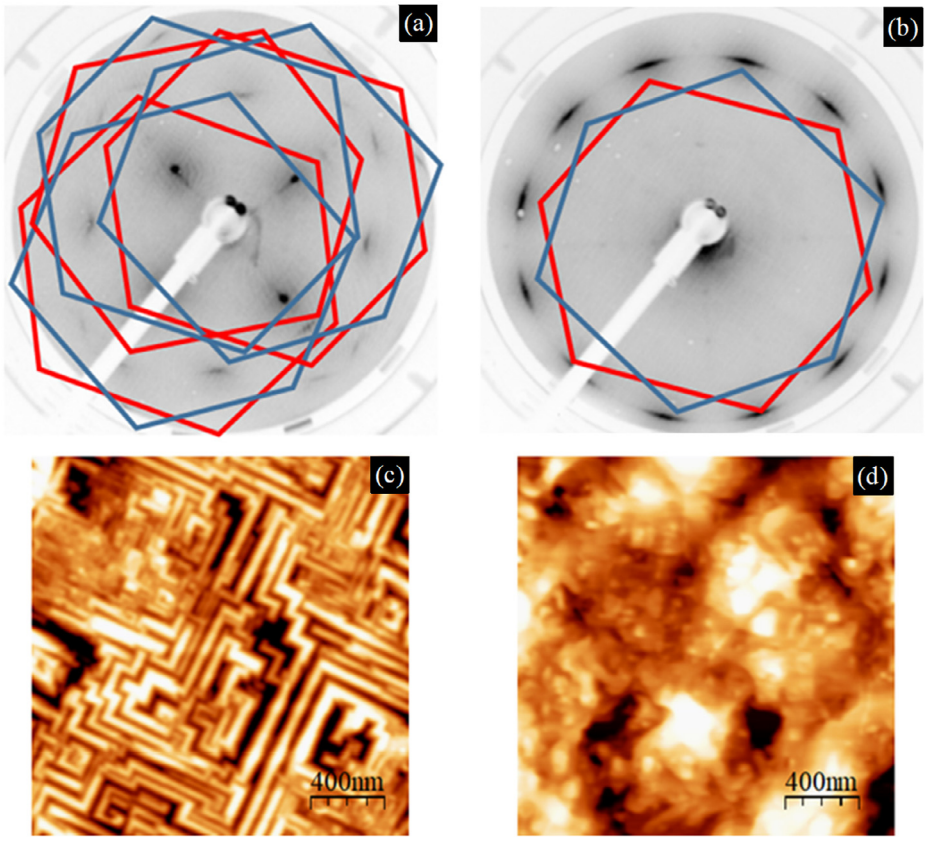

Fig. 2. (a) LEED measurements recorded at 70 eV for graphene/Ge(001) pristine sample, (b) LEED recorded from sample after hydrogen intercalation (c) AFM images of pristine graphene/Ge(001) sample (d) AFM results for graphene/Ge(001) system after hydrogen intercalation.

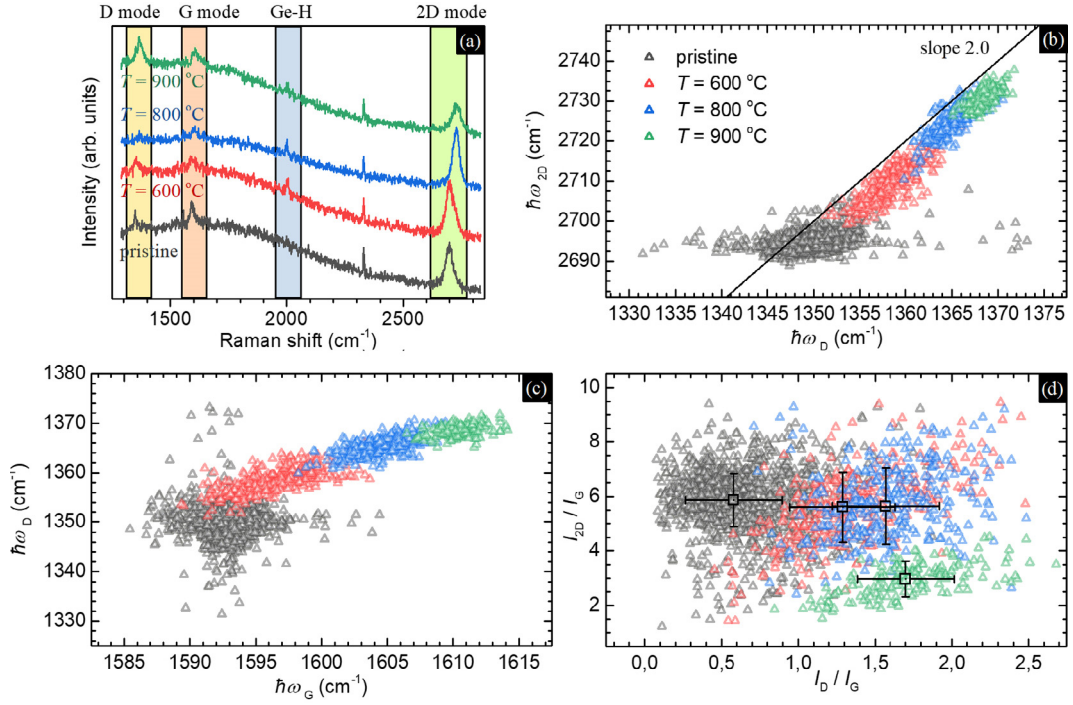

Fig. 3. (a) typical Raman spectra of graphene monolayer on germanium (100) before and after hydrogenation at $T = 600$ °C, 800 °C, and 900 °C. (b) Correlation analysis of Raman 2D mode position versus D mode position. (c) Correlation analysis of Raman D mode position versus G mode position. (d) Correlation analysis of the ratio of the 2D mode intensity to G mode intensity I_{2D}/I_G versus ratio of the D mode intensity versus G mode intensity I_D/I_G.

The main investigation technique which was used in our experiments is Raman spectroscopy. Raman spectra were collected using Renishaw inVia spectrometer with 532 nm laser source, x50 microscope objective (~2 μm laser spot) and using low power (< 0.3 mW) circular light polarization on the sample. Typical Raman spectra acquired from pristine and intercalated graphene samples at $T = 600$ °C, 800 °C, or 900 °C are shown in Fig. 3a. All four spectra include three peaks related to graphene monolayer and are denoted as D mode, G mode, and 2D mode. Three spectra from hydrogenated samples additionally include one peak related to germanium-hydrogen bond, which is denoted as Ge-H (and it is not seen in pristine sample spectrum). The G mode is located approximately at ~1600 cm^{-1} and is a signature of sp^2 carbon vibrations. The D mode is located approximately at ~1350 cm^{-1} and is related to the existence of structural defects [22]. The higher ratio of the D mode intensity to the G mode intensity I_D/I_G, the larger amount of sp^3 defects in sp^2 lattice. The 2D mode is an overtone of the D mode [23–25] but in contrast it is observed even for defect-free samples due to different physical mechanism underlying. It can be observed in graphite, carbon nanotubes and graphene, in case of which, the higher ratio of its intensity to the intensity of the G mode I_{2D}/I_G the higher the structural quality. Because Raman spectra for all samples change within each sample, we acquired not only single Raman spectra but a set of Raman spectra acquired from a square grid of points called Raman maps (~120 spectra in the map), which were subjected to further statistical analysis. Such approach yields results that reflect inhomogeneity of the examined samples and allows for analysis of correlation between different Raman parameters.

Analysis of graphene properties from sets of Raman spectra was performed in a scheme proposed by Lee [9] and is illustrated in Fig. 4a and b. The method of vector decomposition adopted here bases on the fact that changes in Raman peak positions (phonon energies) due to applied stress and doping are different for G and 2D mode. For example Shin [26] reported that changes in the G and 2D mode resulting from compressive biaxial strain give: $\Delta\hbar\omega_G/\Delta\varepsilon = -62\ cm^{-1}/\%$ and $\Delta\hbar\omega_{2D}/\Delta\varepsilon = -138\ cm^{-1}/\%$, thus $\Delta\hbar\omega_{2D}/\Delta\hbar\omega_G = 2.23$. On the other hand, Froehlicher [27] showed that changes in hole doping give $\Delta\hbar\omega_{2D}/\Delta\hbar\omega_G = 0.55$. Because $\Delta\hbar\omega_{2D}/\Delta\hbar\omega_G$ is different for changes in ε and n_h, therefore, it is possible to unambiguously transform ($\hbar\omega_G$, $\hbar\omega_{2D}$) into (ε, n_h).

3. Results and discussion

Prior to a discussion on the influence of the temperature of the hydrogen intercalation on the changes in strain and doping, it is valuable to analyze Raman spectra to get information on introduced structural defects. For this purpose, we analyze D, G, and 2D peak positions, ratio of the intensity of the 2D mode to the intensity of the G mode – I_{2D}/I_G, and the ratio of the intensity of the D mode to the intensity of the G mode – I_D/I_G, which are all depicted in Fig. 3b, c and d. Fig. 3b illustrates distribution of the 2D mode peak positions in respect to the D mode peak positions. The most spread out data are acquired from pristine graphene, which we attribute simply to the lowest intensity of the D mode, which implies higher experimental noise in the peak position. The D and 2D peak positions acquired from hydrogen treated samples are strongly correlated and lie close to the line with slope that equals 2.0. The particular slope value comes from the fact, that 2D mode is an overtone of D mode [23–25]. After analyzing this picture it can be concluded that strain and doping affect D mode in a similar manner to 2D mode. However, for good quality samples, it is more convenient to analyze 2D mode than D mode due to higher intensity. Fig. 3c illustrates distribution of the D mode peak position in respect to the G mode peak position. Fig. 3d illustrates I_{2D}/I_G ratio versus I_D/I_G ratio. We note that the I_D/I_G ratio is related to the amount of defects in graphene monolayer, whereas the I_{2D}/I_G ratio reflects the graphene quality. As can be seen, hydrogen intercalation increases the I_D/I_G ratio from 0.58 ± 0.31 to 1.29 ± 0.34, 1.57 ± 0.35, and 1.70 ± 0.32, for $T = 600$ °C, 800 °C, and 900 °C, respectively. This means that exposition to the hydrogen during cooling increases the amount of sp^3 bonds in respect to the sp^2 bonds. The analysis of the I_{2D}/I_G ratio shows its slight decrease from 6.1 ± 1.0 to 5.6 ± 1.3 and 5.6 ± 1.4, for $T = 600$ °C, 800 °C, respectively, and a large drop in its value to 3.0 ± 0.6 for the highest temperature of 900 °C.

Fig. 4a presents results of the experimental measurements of $\hbar\omega_G$ and $\hbar\omega'_{2D}$ for all four samples in the $\hbar\omega_{2D}$-$\hbar\omega_G$ coordinate system. Because our measurements have been conducted using 532 nm line of ND:YAG laser and most of the literature results, including [26] and [27], was reported to use 514 nm line of Ar laser, in order to be compatible with them and thus to be able to draw reliable conclusions, we modified the $\hbar\omega_{2D}$ values in Fig. 4a assuming that 2D mode in graphene monolayer has dispersion 100 cm^{-1}/eV, after [22]. Additionally, we draw lines of constant strain in $\Delta\varepsilon = 0.05\%$ steps and of constant hole doping from $0 \times 10^{12}\ cm^{-2}$ to $20 \times 10^{12}\ cm^{-2}$ in $n_h = 1 \times 10^{12}\ cm^{-2}$ steps. As the origin (reference) we took data from Ref. [9].

As can be seen in Fig. 4a, energies of G and 2D phonons go up with increasing starting temperature of hydrogenation in a way that reflects the increase in a strain value. Exact numerical values obtained from Raman peak analysis, i.e. median of D, G, and 2D peak positions, as well as the corresponding values of strain and hole doping, are presented in Table 1. Dispersion of analyzed parameters is expressed by means of standard deviation, whereas correlation strength is expressed as the Person correlation coefficient. As it is always valuable to analyze acquired experimental data distribution directly, we transformed Raman data from Fig. 4a into corresponding strain and hole doping values, which are shown in Fig. 4b. Such an approach allows for qualitative

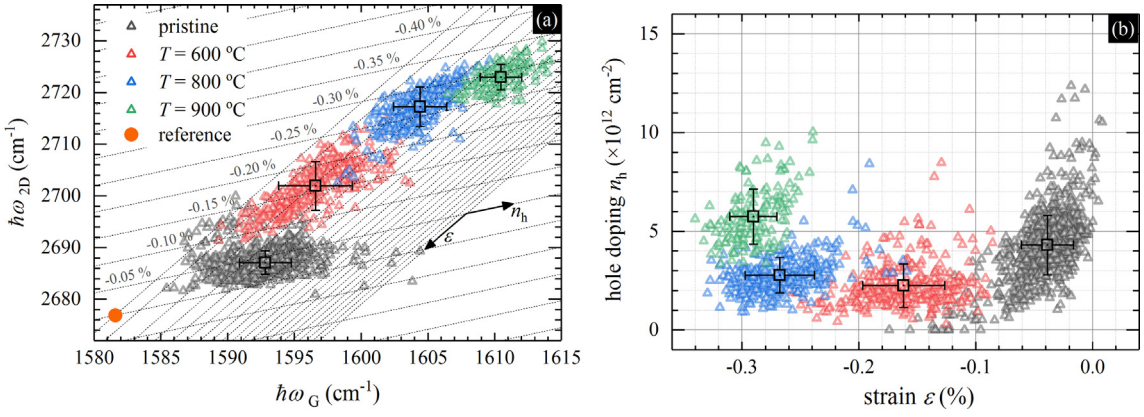

Fig. 4. (a) Correlation analysis of Raman 2D mode position versus G mode position. A shift related to stress increase is clearly seen. (b) Experimental results transformed into stress-doping ε-n coordinate system.

Table 1
Parameters obtained from Raman peak analysis: median of D, G and 2D peak positions; Pearson correlation values ρ between D and G mode positions and between 2D and G mode positions for each temperature of hydrogenation, as well as the derivatives of the 2D mode position with respect to G mode position and D mode position with respect to G mode position obtained using Deming orthogonal regression; mean values of strain and hole doping calculated from Raman data using vector decomposition method; ratio of the intensity of the 2D mode to the intensity of the G mode I_{2D} / I_G; ratio of the intensity of the D mode to the intensity of the G mode I_D / I_G; uncertainties are taken as the standard deviation of the results.

Sample	$\hbar\tilde{\omega}_D$	$\hbar\tilde{\omega}_G$	$\hbar\tilde{\omega}_{2D}$	ρ ($\hbar\omega_D$, $\hbar\omega_G$)	$\partial\hbar\omega_D/\partial\hbar\omega_G$	ρ ($\hbar\omega_{2D}$, $\hbar\omega_G$)	$\partial\hbar\omega_{2D}/\partial\hbar\omega_G$	ε (%)	n_h ($\times 10^{12}$ cm^{-2})	$\tilde{I_D/I_G}$	$\tilde{I_{2D}/I_G}$
Pristine	1349.9	1592.9	2694.8	0	–	0.18	–	−0.04 ± 0.02	4.3 ± 1.5	0.58 ± 0.31	6.1 ± 1.0
T = 600 °C	1358.7	1596.6	2710.1	0.66	0.85	0.79	2.0	−0.16 ± 0.04	2.2 ± 1.1	1.29 ± 0.34	5.6 ± 1.3
T = 800 °C	1365.3	1604.4	2725.4	0.65	0.92	0.76	2.3	−0.27 ± 0.03	2.8 ± 0.9	1.57 ± 0.35	5.6 ± 1.4
T = 900 °C	1368.4	1610.5	2731.2	0.38	0.60	0.57	2.1	−0.29 ± 0.02	5.7 ± 1.4	1.70 ± 0.32	3.0 ± 0.6

assessment of the sample homogeneity, which could provide valuable feedback to the technology. Additionally, it facilitates spotting gross errors. We also note that Fig. 4a is somehow similar to Fig. 3c. The ($\hbar\omega_G$, $\hbar\omega_D$) data could be used for calculations of the strain and doping, like in the case of ($\hbar\omega_G$, $\hbar\omega_{2D}$); however, the original choice [9] seems to be more convenient. We note that data shown in Figs. 3b and c, and 4a are all consistent, which proves that the results reported by us are reliable.

Raman analysis shows that the pristine sample is the least strained one (0.04% of compressive strain). Estimated doping equals approximately 4.3×10^{12} cm^{-2} and its distribution, expressed as the standard deviation, equals 1.5×10^{12} cm^{-2}. Hydrogenation at T = 600 °C results in a decrease in hole doping level (from 4.3×10^{12} cm^{-2} to 2.2×10^{12} cm^{-2}), a decrease in hole doping distribution (from 1.5×10^{12} cm^{-2} to 1.1×10^{12} cm^{-2}) and an increase in compressive strain (from −0.04% to −0.16%). Hydrogen treatment at T = 800 °C results in further increase in compressive strain value (from −0.16% to −0.27%) and in a slight increase in hole doping level (from 2.2×10^{12} cm^{-2} to 2.8×10^{12} cm^{-2}). An increase in hydrogen exposure starting temperature from T = 800 °C to T = 900 °C (close to growth temperature) results in a slight increase in compressive strain (from −0.27% to −0.29%), a large increase in hole doping level (from 2.8×10^{12} to 5.7×10^{12}), and a large increase in hole doping distribution (from 0.9×10^{12} cm^{-2} to 1.5×10^{12} cm^{-2}). We note that large variation in doping values (1.4–1.5 $\times 10^{12}$ cm^{-2}) for samples hydrogenated at T = 600 °C and 900 °C results from existence of correlation between ε and n_h. Both clearly indicate that there is a physical cause that relates ε and n_h. This fact, however, will be discussed further.

Summarizing this part, hydrogen intercalation in T = 600 °C leads to a decrease in hole doping n_h, increase in compressive strain ε, increase in amount of defects and slight decrease in the I_{2D}/I_G ratio. Next, hydrogen treatment in T = 800 °C, leads to a slight increase in hole doping n_h, an increase in compressive strain ε, an increase in the amount of defects and slight decrease in I_{2D}/I_G ratio. Finally, hydrogenation in T = 900 °C leads to large increase in hole doping n_h, a slight increase in compressive strain, slight increase in the amount of defects and large drop in the I_{2D}/I_G ratio.

The interpretation of observed phenomena is as follows. For the pristine sample graphene grown on germanium surface reflects the Ge surface reconstruction, as shown in Fig. 1b and 2c. It has two consequences. The first is that graphene has larger surface area per μm^2 on reconstructed Ge surface than on flat surface, which will be important further. The second is that the graphene is supposed to significantly interact with the germanium surface [28]. We expect that the variation in doping values and an existence of correlation between ε and n_h in pristine graphene is related to the variation in the strength of the coupling to the substrate. We anticipate that the higher coupling between graphene and germanium the higher hole doping resulting in a charge transfer. On the other hand, lower coupling implies that graphene tends to straighten, which in case of graphene excess leads to an increase in compressive strain. We are aware that the complete explanation is not so simple, at least for the fact, that if the graphene monolayer was bound to the substrate at the growth temperature, and the coupling between graphene and germanium surface was strong enough, the strain originating from the thermal coefficient mismatch at room temperature would equal approximately −1.1%, assuming that $\alpha_{Ge} = +6 \times 10^{-6}$ K^{-1} and $\alpha_{GR} = -6 \times 10^{-6}$ K^{-1} [29], whereas the experimental value equals −0.04% ± 0.02%.

Hydrogen intercalation in T = 600 °C and 800 °C leads to crowding of hydrogen between graphene and germanium. Because graphene monolayer cannot be simply straightened due to its excess, therefore it is folding and hence an increase in compressive strain value is expected. This effect can be observed in Fig. 1d, which illustrates graphene sample after hydrogenation. We attribute small bright features exactly to the folded graphene. Moreover, we suppose that hydrogen intercalation decreases in strength of the graphene-germanium interaction, which implies a decrease in the absolute value of the charge carrier concentration. We also note that hydrogenation in T = 600 °C and 800 °C slightly damages graphene monolayer which is related to an increase in the I_D/I_G ratio and a slight decrease in I_{2D}/I_G ratio. Contrary to this, for the sample exposed to hydrogen in T = 900 °C we observe a slight increase the I_D/I_G ratio and a significant decrease in the I_{2D}/I_G ratio, which we attribute with more aggressive etching of the graphene by hydrogen. The drop in the I_{2D}/I_G value is not the only feature that distinguishes the sample hydrogenated in T = 900 °C from samples hydrogenated in T = 600 °C and T = 800 °C. The other ones are: a smaller increase in compressive strain value, a larger increase in hole doping value and emergence of correlation between ε and n_h seen in Fig. 3b. Whereas the first dissimilarity can be explained by the saturation of the hydrogen intercalation, and the second one by the increase in amount of structural defects that could also act as hole dopants, the emergence of correlation between ε and n_h escapes our understanding at the moment.

4. Conclusions

To conclude, we have demonstrated the role of hydrogen intercalation on graphene structural properties, namely the impact of hydrogen on the amount of structural defects and on an increase in value of compressive strain acting on graphene monolayer. The latter one results from the fact that initially graphene mimics reconstructed germanium surface. Hydrogen intercalation leads to decoupling of carbon film from germanium which in case of graphene excess leads to an increase in compressive strain. The initial decrease in hole doping and its significant increase for the most damaged sample is also discussed. Aforementioned information and conclusions provide deeper insight into graphene-germanium interaction and could be used for further improvement of graphene on germanium growth technology.

Acknowledgements

IP and WS would like to thank the National Science Centre, Poland, for financial support within Project No. 2016/23/D/ST5/00633. JJ would like to thank the National Science Centre, Poland, for financial support within Project No. 2014/15/D/ST5/03944. P. D. was supported by the National Science Centre, Poland, Grant No. 2015/19/D/ST5/

01933. MZ acknowledges the support by the EU Graphene Flagship funding (Grant Graphene Core2 785219). We would like to thank J. Grzonka for help with the SEM images.

References

[1] X.S. Li, W.W. Cai, J.H. An, S. Kim, J. Nah, D.X. Yang, R. Piner, A. Velamakanni, I. Jung, E. Tutuc, S.K. Banerjee, L. Colombo, R.S. Ruoff, Large-area synthesis of high-quality and uniform graphene films on copper foils, Science 324 (2009) 5932.

[2] G. Lupina, J. Kitzmann, I. Costina, M. Lukosius, C. Wenger, A. Wolff, S. Vaziri, M. Ostling, I. Pasternak, A. Krajewska, W. Strupinski, S. Kataria, A. Gahoi, M.C. Lemme, G. Ruhl, G. Zoth, O. Luxenhofer, W. Mehr, Residual metallic contamination of transferred chemical vapor deposited graphene, ACS Nano 9 (2015) 4776.

[3] J.-H. Lee, E.K. Lee, W.-J. Joo, Y. Jang, B.-S. Kim, J.Y. Lim, S.-H. Choi, S.J. Ahn, J.R. Ahn, M.-H. Park, C.-W. Yang, B.L. Choi, S.-W. Hwang, D. Whang, Wafer-scale growth of single-crystal monolayer graphene on reusable hydrogen-terminated germanium, Science 344 (2014) 286.

[4] G. Wang, M. Zhang, Y. Zhu, G. Ding, D. Jiang, Q. Guo, S. Liu, X. Xie, P.K. Chu, Z. Di, X. Wang, Direct growth of graphene film on germanium substrate, Sci. Rep. 3 (2013) 2465.

[5] G. Lippert, J. Dabrowski, T. Schroeder, M.A. Schubert, Y. Yamamoto, F. Herziger, J. Maultzsch, J. Baringhaus, C. Tegenkamp, M.C. Asensio, J. Avila, G. Lupina, Graphene grown on Ge (001) from atomic source, Carbon 75 (2014) 104.

[6] B. Kiraly, R.M. Jacobberger, A.J. Mannix, G.P. Campbell, M.J. Bedzyk, M.S. Arnold, M.C. Hersam, N.P. Guisinger, Electronic and mechanical properties of graphene – germanium interfaces grown by chemical vapor deposition, Nano Lett. 15 (2015) 7414.

[7] I. Pasternak, M. Wesolowski, I. Jozwik, M. Lukosius, G. Lupina, P. Dabrowski, J.M. Baranowski, W. Strupinski, Graphene growth on Ge(100)/Si(100) substrates by CVD method, Sci. Rep. 6 (2016) 21773.

[8] C. Riedl, C. Coletti, T. Iwasaki, A.A. Zakharov, U. Starke, Quasi-free-standing epitaxial graphene on SiC obtained by hydrogen intercalation, Phys. Rev. Lett. 103 (2012) 246804.

[9] J.E. Lee, G. Ahn, J. Shim, Y.S. Lee, S. Ryu, Optical separation of mechanical strain from charge doping in graphene, Nat. Commun. 3 (2012) 1024.

[10] M. Lukosius, J. Dabrowski, J. Kitzmann, O. Fursenko, F. Akhtar, M. Lisker, et al., Metal-free CVD graphene synthesis on 200 mm Ge/Si(001) substrates, ACS Appl. Mater. Interfaces 8 (2016) 33786–33793.

[11] I. Pasternak, P. Dabrowski, P. Ciepielewski, V. Kolkovsky, Z. Klusek, J.M. Baranowski, W. Strupinski, Large-area high-quality graphene on Ge(001)/Si (001) substrates, Nanoscale 8 (2016) 11241–11247.

[12] A.M. Scaparro, V. Miseikis, C. Coletti, A. Notargiacomo, M. Pea, M. De Seta, L. Di Gaspare, ACS Appl. Mater. Interfaces 8 (2016) 33083–33090.

[13] P. Dabrowski, M. Rogala, I. Pasternak, J. Baranowski, W. Strupinski, M. Kopciuszynski, R. Zdyb, M. Jalochowski, I. Lutsyk, Z. Klusek, The study of the interactions between graphene and Ge(001)/Si(001), Nano Res. 10 (2017) 3648–3661.

[14] Shinichi Tanabe, Makoto Takamura, Yuichi Harada, Hiroyuki Kageshima, Hiroki hibino effects of hydrogen intercalation on transport properties of quasi-free-standing monolayer graphene Jpn, J. Appl. Phys. 53 (2014).

[15] Y. Anno, Y. Imakita, K. Takei, S. Akita, T. Arie, Enhancement of graphene thermoelectric performance through defect engineering, 2D Mater. 4 (2017) 025019.

[16] A. Mani, C. Benjamin, Strained-graphene-based highly efficient quantum heat engine operating at maximum power, Phys. Rev. E 96 (2017) 032118.

[17] N.J.G. Couto, D. Costanzo, S. Engels, D.-K. Ki, K. Watanabe, T. Taniguchi, C. Stampfer, F. Guinea, A.F. Morpurgo, Random strain fluctuations as dominant disorder source for high-quality on-substrate graphene devices, Phys. Rev. X 4 (2014) 041019.

[18] K.M. McElhinny, R.M. Jacobberger, A.J. Zaug, M.S. Arnold, P.G. Evans, Graphene-induced Ge (001) surface faceting, Surf. Sci. 647 (2016) 90.

[19] M. Lukosius, J. Dabrowski, J. Kitzmann, O. Fursenko, F. Akhtar, M. Lisker, G. Lippert, S. Schulze, Y. Yamamoto, M.A. Schubert, H.M. Krause, A. Wolff, A. Mai, T. Schroeder, G. Lupina, Metal-free CVD graphene synthesis on 200 mm Ge/Si(001) substrates, ACS Appl. Mater. Interfaces 8 (2016) 33786.

[20] I. Pasternak, P. Dabrowski, P. Ciepielewski, V. Kolkovsky, Z. Klusek, J.M. Baranowski, W. Strupinski, Large-area high-quality graphene on Ge(001)/Si (001) substrates, Nanoscale 8 (2016) 11241.

[21] J. Grzonka, I. Pasternak, P.P. Małachowski, V. Kolkowsky, W. Strupiński, Influence of hydrogen intercalation on graphene/Ge(001)/Si(001) interface, Appl. Surf. Sci. 447 (2018) 582.

[22] A.C. Ferrari, J. Robertson, Interpretation of Raman spectra of disordered and amorphous carbon, Phys. Rev. B 61 (2000) 14095.

[23] A.C. Ferrari, J.C. Meyer, V. Scardaci, C. Casiraghi, M. Lazzeri, F. Mauri, S. Piscanec, D. Jiang, K.S. Novoselov, S. Roth, A.K. Geim, Raman spectrum of graphene and graphene layers, Phys. Rev. Lett. 97 (2006) 187401.

[24] L.M. Malard, J. Nilsson, D.C. Elias, J.C. Brant, F. Plentz, E.S. Alves, A.H. Castro Neto, M.A. Pimenta, Probing the electronic structure of bilayer graphene by Raman scattering, Phys. Rev. B 76 (2007) 201401.

[25] P. Venezuela, M. Lazzeri, F. Mauri, Theory of double-resonant Raman spectra in graphene: intensity and line shape of defect-induced and two-phonon bands, Phys. Rev. B 84 (2011) 035433.

[26] Y. Shin, M. Lozada-Hidalgo, J.L. Sambricio, I.V. Grigorieva, A.K. Geim, C. Casiraghi, Raman spectroscopy of highly pressurized graphene membranes, Appl. Phys. Lett. 108 (2016) 221907.

[27] G. Froehlicher, S. Berciaud, Raman spectroscopy of electrochemically gated graphene transistors: geometrical capacitance, electron-phonon, electron-electron, and electron-defect scattering, Phys. Rev. B 91 (2015) 205413.

[28] P. Dąbrowski, M. Rogala, I. Pasternak, J. Baranowski, W. Strupiński, M. Kopciuszyński, R. Zdyb, M. Jalochowski, I. Lutsyk, Z. Klusek, The study of the interactions between graphene and Ge(001)/Si(001), Nano Res. 10 (2017) 3648.

[29] D. Yoon, Y.W. Son, H. Cheong, Negative thermal expansion coefficient of graphene measured by Raman spectroscopy, Nano Lett. 11 (2011) 3227.